On the Relationship between Parametric and Geometric Active Contours

Chenyang Xu*, Anthony Yezzi, Jr.†, and Jerry L. Prince*
*Center for Imaging Science, ECE Department, The Johns Hopkins University, Baltimore, MD 21218
†School of Electrical and Computer Engineering, Georgia Institute of Technology, Atlanta, GA 30332

Technical Report JHU/ECE 99-14, December 3, 1999

Abstract

There are currently two main types of active contours: 1) parametric active contours, which represent contours explicitly as parameterized curves; and 2) geometric active contours, which represent contours implicitly as level sets of two-dimensional scalar functions. In this paper, we derive an explicit mathematical relationship between the general formulations of parametric and geometric active contours. Based on this relationship and the results of two recent parametric active contours, we propose two new geometric active contours. Using both simulated and real images, we show that the proposed algorithms have an improved performance over both existing parametric and geometric active contours.

1 Introduction

Active contours [9], a physically-motivated model that can deform itself to recover object shape from digital images, have been extensively researched in the past decade (see [14] for a recent survey on this topic). Current active contours can be classified as either *parametric active contours* (cf. [9, 2, 7]) or *geometric active contours* (cf. [4, 12, 5, 25]) according to the contour representation they used. Parametric active contours, which are physically motivated [9, 22], represent contours explicitly as parameterized curves, whereas geometric active contours, based on the theory of curve evolution [19, 1, 11] and implemented via level set techniques [15], represent curves implicitly as level sets of two-dimensional scalar functions.

The importance of understanding the relationship between parametric and geometric formulations of active contours has been recognized. Caselles *et al.* [6] showed that their proposed geometric active contours are equivalent to the classical parametric active contours. Aubert and Blanc-Féraud [3] revisited this equivalence and extended it to the 3-D (active surface) case. However, the equivalence they have shown is limited to the active contours derived from energy minimization only, thus the question of whether the geometric formulation can be found for the more general active contours, such as those using non-conservative external forces [24], is not addressed.

In this paper, we show that an explicit mathematical relationship between the general formulations of parametric and geometric active contours can be derived using the curve evolution theory. Based on this relationship and the results of two recent parametric active contours, we propose two new geometric active contours. Using both simulated and real images, we show that the proposed algorithms have an improved performance over both existing parametric and geometric active contours.

2 Background

In this section, we review the relevant background information about parametric and geometric active contours and comment on their advantages and limitations.

2.1 Parametric active contours

The classical parametric active contours, proposed by Kass *et al.* [9], are formulated by minimizing an energy functional that takes a minimum when contours are smooth and reside on object boundaries. Solving the energy minimization problem leads to a dynamic equation that has both internal and external forces. The external forces resulting from this formulation are conservative forces in that they can be written as gradients of scalar potential functions. Active contours using non-conservative forces, however, have been shown to have improved performance over traditional energy-minimizing active contours (see [24, 23]). In this section, we describe a more general formulation that is derived directly from Newton's law, allowing the use of either conservative or non-conservative forces.

Please address correspondence to *prince@jhu.edu*.

Mathematically, a parametric active contour is a time-varying curve $\boldsymbol{X}(s,t) = [X(s,t), Y(s,t)]$ where $s \in [0,1]$ is a parameterization and $t \in \mathbf{R}^+$ is the time. The dynamics of the curve are governed by Newton's second law which takes the following form

$$\mu \frac{\partial^2 \boldsymbol{X}}{\partial t^2} = \boldsymbol{F}_{\rm damp}(\boldsymbol{X}) + \boldsymbol{F}_{\rm int}(\boldsymbol{X}) + \boldsymbol{F}_{\rm ext}(\boldsymbol{X}) \,, \quad (1)$$

where μ is a coefficient with units of mass, and $\boldsymbol{F}_{\rm damp}(\boldsymbol{X})$, $\boldsymbol{F}_{\rm int}(\boldsymbol{X})$, and $\boldsymbol{F}_{\rm ext}(\boldsymbol{X})$ are the *damping* (or viscous), *internal*, and *external forces*, respectively.

The damping force is defined as

$$\boldsymbol{F}_{\rm damp} = -\gamma \frac{\partial \boldsymbol{X}}{\partial t} \,, \quad (2)$$

where γ is the damping coefficient. The internal force is derived from an internal deformation energy [9], and is given by

$$\boldsymbol{F}_{\rm int}(\boldsymbol{X}) = \frac{\partial}{\partial s}\left(\alpha \frac{\partial \boldsymbol{X}}{\partial s}\right) - \frac{\partial^2}{\partial s^2}\left(\beta \frac{\partial^2 \boldsymbol{X}}{\partial s^2}\right) \,, \quad (3)$$

where the weighting parameters $\alpha(s)$ and $\beta(s)$ can be used to control the strength of the contour's tension and rigidity, respectively. In practice, $\alpha(s)$ and $\beta(s)$ are often set to constants.

The external force is designed to pull an active contour towards object boundaries or other features of interest. The design of external forces is crucial since they directly determine the accuracy and performance of active contours. Many types of external forces have been developed in the past including the well-known pressure force [7] and the Gaussian potential force [9]. The pressure force is given by

$$\boldsymbol{F}_p(\boldsymbol{X}) = w_p \boldsymbol{N}(\boldsymbol{X}) \,, \quad (4)$$

where w_p is a scalar and $\boldsymbol{N}(\boldsymbol{X})$ is the unit normal to the contour $\boldsymbol{X}$. In this paper, we define $\boldsymbol{N}(\boldsymbol{X})$ to be the inward unit normal of the contour.

The Gaussian potential force is defined on the entire image domain and is given by

$$\boldsymbol{F}_g(\boldsymbol{x}) = -\nabla P(\boldsymbol{x}) \,, \quad (5)$$

where $\boldsymbol{x}$ is any location in an image $I(\boldsymbol{x})$, and $P(\boldsymbol{x})$, a potential function that takes minimum at step edges or/and lines, is defined as

$$P(\boldsymbol{x}) = -w_e |\nabla [G_\sigma(\boldsymbol{x}) * I(\boldsymbol{x})]|^2 + w_l [G_\sigma(\boldsymbol{x}) * I(\boldsymbol{x})] \,, \quad (6)$$

where $G_\sigma(\boldsymbol{x})$ is a 2-D Gaussian function with standard deviation σ, ∇ is the gradient operator, $*$ is the 2-D image convolution operator, and w_e and w_l are weighting parameters for edges and lines, respectively.

We note that the mass coefficient μ is often set to zero in practice because it requires more storage and may also cause oscillations near object boundaries. Putting all the usual assumptions together, we find that the typical dynamic active contour equations are given by

$$\gamma \frac{\partial \boldsymbol{X}}{\partial t} = \frac{\partial}{\partial s}\left(\alpha \frac{\partial \boldsymbol{X}}{\partial s}\right) - \frac{\partial^2}{\partial s^2}\left(\beta \frac{\partial^2 \boldsymbol{X}}{\partial s^2}\right) + \boldsymbol{F}_{\rm ext}(\boldsymbol{X}) \,. \quad (7)$$

Parametric active contours have been applied successfully in a wide range of applications (cf. [7, 21, 8, 24]). They have two limitations due to their parametric representation, however. First, it is often necessary to dynamically reparameterize the active contour in order to maintain a faithful delineation of the object boundary. This leads to additional algorithm complexity and computational overhead. The second limitation of the parametric approach is that topological adaptation is difficult. In particular, the splitting or merging of model parts requires a new topology and the construction of a new parameterization. Sophisticated schemes have been developed for this purpose [8, 13], but these add to the algorithm complexity and computational burden as well.

2.2 Geometric active contours

Geometric active contours, proposed independently by Caselles *et al.* [4] and Malladi *et al.* [12], provide an elegant solution to address the limitations of parametric active contours described in the previous section. The formulation of geometric active contours is based on curve evolution theory [19, 11, 1] and the level set method [15]. In this framework, curves are evolved using only geometric measures, resulting in a contour evolution that is independent of the parameterization. As a result, one or multiple evolving contours can be represented implicitly as a level set of a 2-D scalar function and their parameterizations are computed only after the deformation, thereby allowing both reparameterization and topology adaptation to be handled automatically.

We now briefly describe the formulation and limitations of several representative geometric active contours. Given a 2-D scalar function $\phi(\boldsymbol{x}, t)$ that embeds the contour of interest as its zero level set, the geometric active contour formulation, proposed by Caselles *et al.* [4] and Malladi *et al.* [12], takes the following form

$$\frac{\partial \phi}{\partial t} = c(\kappa + V_0)|\nabla \phi| \,, \quad (8)$$

where κ is the level set curvature, V_0 is a constant, and

$$c \equiv c(\boldsymbol{x}) = \frac{1}{1 + |\nabla [G_\sigma(\boldsymbol{x}) * I(\boldsymbol{x})]|} \,. \quad (9)$$

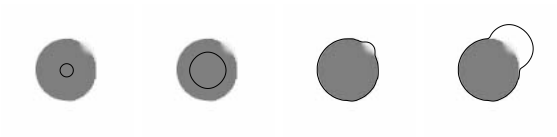

Figure 1. A geometric active contour using constant expansion term can leak out weak boundary, yielding unreliable results.

In (8), the product $c(\kappa + V_0)$ determines the overall evolution speed of level sets of $\phi(\boldsymbol{x}, t)$ along their normal direction. The use of curvature κ has the effect of smoothing the contour, while the use of V_0 has the effect of shrinking or expanding contour at a constant speed. The speed of contour evolution is coupled with the image data through a multiplicative stopping term c.

This scheme works well for objects that have good contrast. However, when the object boundary is indistinct or has gaps, this type of geometric active contours may leak out because the multiplicative term only slows down the contour near the boundary rather than completely stopping the contour. Once the contour passes the boundary, it will not be pulled back to recover the desired boundary.

To remedy this problem, Caselles *et al.* [5, 6] and Kichenassamy *et al.* [10, 25] proposed the following formulation

$$\frac{\partial \phi}{\partial t} = c(\kappa + V_0)|\nabla \phi| + \nabla c \cdot \nabla \phi \; . \tag{10}$$

The extra stopping term $\nabla c \cdot \nabla \phi$ is used to pull back the contour if it passes the boundary. As noted by Siddiqi *et al.* [20], however, this formulation is still subject to the boundary leaking problem.

To further address the boundary leaking problem, Siddiqi *et al.* [20] proposed the following formulation

$$\frac{\partial \phi}{\partial t} = (c\kappa|\nabla \phi| + \nabla c \cdot \nabla \phi) + V_0(c + \frac{1}{2}\boldsymbol{X} \cdot \nabla c)|\nabla \phi| \; . \tag{11}$$

We see that (11) has the additional term $V_0(\boldsymbol{X} \cdot \nabla c)|\nabla \phi|/2$, which provides extra stopping power that can prevent the contour from leaking through small boundary gaps. As noted by the authors, however, these active contours can still leak through boundary gaps when the gaps are large.

To illustrate the boundary leaking problem, we reproduced one of the experiments performed in [20] using a simulated image consisting of a disk with a blurry boundary segment. As shown in Fig. 1, a typical geometric active contour leaks through this blurry boundary segment. Note that although it is possible to carefully tune the value of V_0 in this example to avoid boundary leaking, we found the value of constant expanding/shrinking term V_0 is very sensitive to the edge strength variation in general. A weak edge at a single site is enough to allow the contour to leak, leading to unpredictable results.

The boundary leaking problem in geometric active contours is caused by the constant expanding/shrinking term, which plays a similar role as the pressure force in parametric active contours. This problem has been addressed recently in the parametric active contour literature [18, 17, 24]. The described solutions are able to move an active contour to the desired object boundaries from a long range without leaking through boundary gaps. It is not immediately apparent, however, how these solutions can be adapted to the geometric active contour framework. In this paper, we make this connection explicit by deriving a mathematical relationship between parametric and geometric active contours. We then show how two new geometric active contours can be obtained through this relationship, and we demonstrate how the boundary leaking problem is solved using these new active contour models.

3 Relationship between parametric and geometric active contours

In this section, we reformulate (7) as a geometric active contour. First, we note that Caselles *et al.* [6] showed that the rigidity term in (7) does not affect the performance of geometric active contours. Therefore, we drop the term associated with β. Second, pressure forces are treated differently than other forces in the geometric active contour formulation because they can cause singularities during deformation. We therefore choose to separate pressure forces $\boldsymbol{F}_p(\boldsymbol{X})$ from other external forces $\boldsymbol{F}_{\text{ext}}(\boldsymbol{X})$. With these two modifications, the class of parametric active contours we consider is described by the following dynamic equation

$$\gamma \frac{\partial \boldsymbol{X}}{\partial t} = \frac{\partial}{\partial s}\left(\alpha \frac{\partial \boldsymbol{X}}{\partial s}\right) + \boldsymbol{F}_p(\boldsymbol{X}) + \boldsymbol{F}_{\text{ext}}(\boldsymbol{X}) \; , \tag{12}$$

To make the evolution (12) geometric, i.e., invariant to changes in the parameterization of $\boldsymbol{X}$, we consider s to be the arc-length parameter in the following discussion.

We consider pressure forces defined by

$$\boldsymbol{F}_p(\boldsymbol{X}) = w_p(\boldsymbol{X})\boldsymbol{N}(\boldsymbol{X}) \; , \tag{13}$$

where w_p is allowed to be spatial-varying function. This is a more general class of pressure forces than the pressure force proposed by Cohen in [7], where w_p is assumed to be a constant. This more general force is easy to implement, however, and can dramatically improve the performance of an active contour, as will be demonstrated in Section 4.1.

We now derive a geometric formulation for (12). We first recall a fundamental relationship between curve evolution

and level set evolution. As derived in [15], the following curve evolution

$$\frac{\partial \boldsymbol{X}}{\partial t} = V(\kappa)\boldsymbol{N} \ , \tag{14}$$

where $\boldsymbol{N}$ is the inward unit normal, can be reformulated as the following level set evolution equation

$$\frac{\partial \phi}{\partial t} = V(\kappa)|\nabla \phi| \ , \tag{15}$$

where the curve of interest is embedded as the zero level set of $\phi(\boldsymbol{x}, t)$. Hence, if we can recast the formulation (12) into the standard curve evolution form defined in (14), we can straightforwardly obtain the corresponding geometric formulation using (15). A key observation here is that in order to represent the curve evolution in level set representation, the curve dynamics should depend only on geometric measures such as the unit normal and curvature.

Since it is known that a contour's tangential motion only affects its parameterization but not its geometry, we modify (12) by considering only the normal components of internal and external forces. Note that the following property holds for $\boldsymbol{X}(s,t)$

$$\frac{\partial}{\partial s}\left(\alpha \frac{\partial \boldsymbol{X}}{\partial s}\right) \cdot \boldsymbol{N} = \alpha\kappa \ ,$$

where κ is the curvature. We can therefore rewrite (12) as follows

$$\frac{\partial \boldsymbol{X}}{\partial t} = (\epsilon\kappa + V_p + \boldsymbol{V}_{\text{ext}} \cdot \boldsymbol{N})\boldsymbol{N} \ , \tag{16}$$

where $\epsilon = \alpha/\gamma$, $V_p = w_p/\gamma$, and $\boldsymbol{V}_{\text{ext}} = \boldsymbol{F}_{\text{ext}}/\gamma$. Here, we have divided through by γ to make both sides have units of velocity.

Equation (16) is in the form of (14) with speed function $V(\kappa) = \epsilon\kappa + V_p + \boldsymbol{V}_{\text{ext}} \cdot \boldsymbol{N}$. Therefore, using this speed function, Equation (15) is the equivalent level set formulation. For further simplification, we note that in the level set representation, the normal $\boldsymbol{N}$ can be calculated using

$$\boldsymbol{N} = -\frac{\nabla \phi}{|\nabla \phi|} \ .$$

Putting these facts together yields the following geometric active contour evolution equation

$$\frac{\partial \phi}{\partial t} = V(\kappa)|\nabla \phi| = (\epsilon\kappa + V_p)|\nabla \phi| - \boldsymbol{V}_{\text{ext}} \cdot \nabla \phi \ . \tag{17}$$

which is equivalent to (12).

We note that V_p is a function defined on the image domain and $\boldsymbol{V}_{\text{ext}}$ has the meaning of a passive convection velocity field in fluid dynamics (see [15]). The geometric evolution equation (17) can be implemented using a fast method (narrow-band algorithm) proposed by Malladi *et al.* [12]. Note that although we distinguish the term *force* from the term *speed* throughout the above derivation, we will use them interchangeably in the following sections since they have the same meaning from a numerical implementation perspective.

4 Two new geometric active contours

This section shows the application of the mathematical relationship derived in Section 3 for designing new geometric active contours based on two recent parametric active contours.

4.1 Region-based geometric active contours

Most geometric active contours use only edge information to guide the active contour to its final destination. When region information is also available — e.g., from image segmentation — this information can be used to improve the robustness of the active contour. Here, we examine a class of region-based parametric active contours proposed by Ronfard [18] and Poon *et al.* [17] and show how they can be reformulated as geometric active contours to improve their overall performance.

The essence of the region-based parametric active contours described in [18, 17] is to modulate the sign of pressure forces using region information so that the contour shrinks when it is outside the object of interest and expands when it is inside the object. We refer to this kind of pressure forces as *signed pressure forces* and the usual pressure forces used in the literature as *unsigned pressure forces* to differ them from each other.

The form of region-based parametric active contours we are interested in is given by

$$\gamma \frac{\partial \boldsymbol{X}}{\partial t} = \frac{\partial}{\partial s}\left(\alpha \frac{\partial \boldsymbol{X}}{\partial s}\right) + w_R R(\boldsymbol{X})\boldsymbol{N}(\boldsymbol{X}) + \boldsymbol{F}_{\text{ext}}(\boldsymbol{X}) \ , \tag{18}$$

where $\boldsymbol{N}(\boldsymbol{X})$ is the inward unit normal of the contour, $R(\boldsymbol{X})$ is computed by evaluating the *region indicator function* $R(\boldsymbol{x})$ evaluated along the contour $\boldsymbol{X}(s,t)$, w_R is a positive weighting parameter, and $\boldsymbol{F}_{\text{ext}}(\boldsymbol{X})$ is the additional external force that may be used. The region indicator function, derived from image intensities, takes value in the range [-1,1]. Its sign is defined to be negative inside the object of interest and positive outside. There are various methods to construct a region indicator function; we will present one method later in this section. Using (12) and (17), we can easily formulate a class of region-based geometric active contours as follows

$$\frac{\partial \phi}{\partial t} = (\epsilon\kappa + w_R/\gamma R)|\nabla \phi| - \boldsymbol{V}_{\text{ext}} \cdot \nabla \phi \ . \tag{19}$$

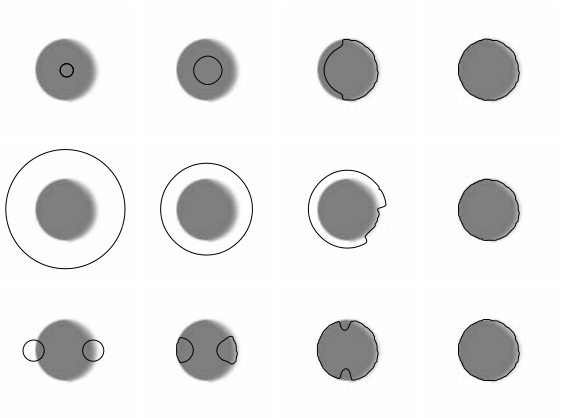

Figure 2. Geometric active contours using signed pressure force are robust to the presence of weak boundaries as demonstrated by the results on a simulated image with three different initializations. The progress of deformation is plotted from left to right for each initialization.

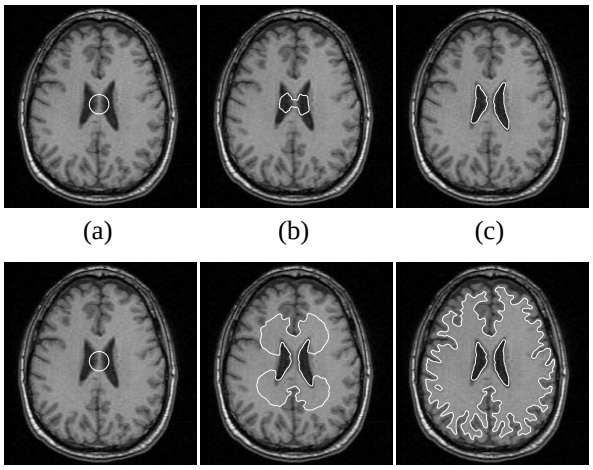

Figure 3. From a single initialization, a region-based geometric active contour can automatically adapt its topology to extract the boundary of either ventricles (top row) or the white matter (bottom row) from an MR brain image according to the selected region indicator function.

To demonstrate the performance of region-based geometric active contours, we carried out a series of experiments on both simulated and real images. In all experiments, we construct the region indicator function automatically using an implementation of fuzzy classification algorithm described in [16] to automatically classify an image into multiple membership functions. The membership functions, defined on each image pixel, provide a soft segmentation based on image intensities. Each membership takes a value between 0 and 1. A pixel with a high value in a particular membership function has a high likelihood to be in that class. Assuming the object foreground has higher values in a particular membership function $\mu_f(\boldsymbol{x})$, then the region indicator function is given by

$$R(\boldsymbol{x}) = 1 - 2\mu_f(\boldsymbol{x}) \; . \tag{20}$$

It is easy to see that the value of $R(\boldsymbol{x})$ is in the range of $[-1, 1]$ and is negative inside the object and positive outside the object, thus satisfying the requirement of being a region indicator function. Note that in the following experiments, we also use an additional external force given by

$$\boldsymbol{F}_{\text{ext}} = \nabla \mu_f(\boldsymbol{x}) \; .$$

Fig. 2 shows an object similar to that of Fig. 1 except that here the blurry region is expanded to the entire right side boundary of the disk. The rows of Fig. 2 show the results of region-based geometric active contours starting from three different initializations. Despite the increased blur region along the boundary, the resulting geometric active contour is completely immune to the boundary leaking problem due to the use of the extra region information. We notice that because of this robustness, higher weights can be used to significantly increase the speed of convergence. Furthermore, the region-based geometric active contours also enjoys an improved robustness to various initializations, in particular, it can now be initialized across the boundary and still converges to the correct result as shown in the bottom row of Fig. 2. Notice that the final extracted boundary contours from three different initializations are almost indistinguishable.

We also applied the region-based geometric active contours to a magnetic resonance (MR) brain image. Fig. 3 shows that from a single initialization, a region-based geometric active contour can automatically adapt its topology to extract the boundary of either the ventricles or the white matter depending on the region indicator function provided. In this experiment, a three-class fuzzy clustering is performed with background pixels discarded, yielding three membership functions for ventricles, gray matter, and white matter tissue classes. Two region indicator functions are then computed for both the ventricles and the white matter according to (20).

4.2 Geometric GVF active contours

The geometric active contour formulation derived in Section 3 allows us to use a non-conservative vector field as its passive convection velocity field. An example of a non-conservative vector field used by the parametric active

contours is the *gradient vector flow* (GVF) field proposed by Xu and Prince [24]. The use of GVF has been shown to have larger capture range and ability to converge into boundary concavities. However, it was only used previously in parametric active contours [24, 23]. Coupling the GVF with geometric active contours has two advantages. First, it improves upon the parametric GVF active contours by allowing automatic topology adaptation. Second, it is not as susceptible to boundary leaking as the existing geometric active contours. Finally, we note that it compliments region-based geometric active contours by being able to work directly with an edge map when region information is not available or cannot be reliably estimated.

A GVF field is defined as the equilibrium solution of a generalized vector diffusion equation

$$\frac{\partial \boldsymbol{v}}{\partial t} = g(|\nabla f|)\nabla^2 \boldsymbol{v} - h(|\nabla f|)(\boldsymbol{v} - \nabla f) \;, \qquad (21)$$

where $\boldsymbol{v}(\boldsymbol{x}, 0) = \nabla f$, $\partial \boldsymbol{v}/\partial t$ denotes the partial derivative of $\boldsymbol{v}(\boldsymbol{x}, t)$ with respect to t, ∇^2 is the Laplacian operator (applied to each spatial component of $\boldsymbol{v}$ separately), and f is an edge map that has higher value at the desired object boundary and can be derived using any edge detector. Note that t is independent of the time variable used in (17). The functions $g(r)$ and $h(r)$ are spatially varying weights that control the amount of diffusion in GVF. In this paper, we choose

$$\begin{aligned} g(r) &= \exp\{-(r/\kappa)^2\} \\ h(r) &= 1 - g(r) \;, \end{aligned}$$

where κ is a scalar and r is a dummy variable.

Using (12) and (17) and excluding the pressure force, we obtain the following evolution equation for geometric GVF active contours

$$\frac{\partial \phi}{\partial t} = \epsilon\kappa - \tilde{\boldsymbol{v}} \cdot \nabla\phi \;, \qquad (22)$$

where $\tilde{\boldsymbol{v}}$ can be either the GVF field itself or the GVF field normalized by its magnitude at nonzero locations. Fig. 4 shows an example in which a geometric GVF active contour was applied to a simulated image containing an object that has both boundary gaps and concavities. In Fig. 4(a), a contour is initialized across the object boundary. Figs. 4(b) and 4(c) plot the contour deforming towards the desired object boundary. The final result shown in Fig. 4(d) demonstrates the ability of the geometric GVF active contour to recover the boundary reliably in the presence of both boundary concavities and gaps.

Fig. 5 shows the result of applying a geometric GVF active contour to segment the left ventricle (LV) of a human heart from an MR image. The original image and its computed edge map are shown in Figs. 5(a) and 5(b), respectively. Figs. 5(c)-(f) show two contours initialized within the LV merge automatically to extract the inner wall of the LV. Notice that a good result is obtained despite the presence of both image noise and weak boundaries (near top and right along the LV inner wall as shown in the edge map).

(a) (b) (c) (d)

Figure 4. A geometric GVF active contour is initialized across the object boundary in a simulated image (a) and deforms into the desired object shape by simultaneously detecting boundary concavities and bridging boundary gaps (b)-(d).

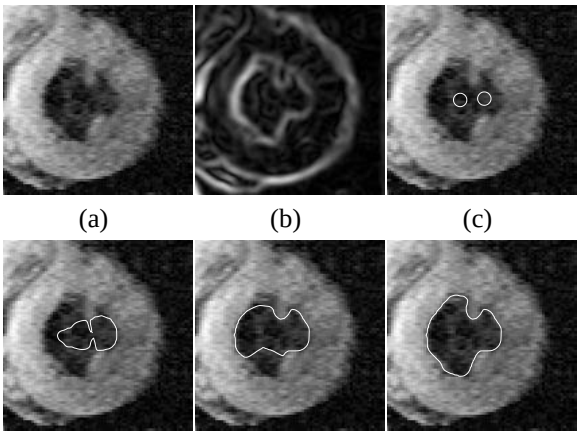

(a) (b) (c)

(d) (e) (f)

Figure 5. Segmentation of the left ventricle (LV) of a human heart using multiple geometric GVF active contours. The MR image of the LV (a) and its computed edge map (b). Two initial contours (c) merge and extract the inner wall of the LV (d)-(e).

We also applied the geometric GVF active contour on a noisy ultrasound cardiac image as shown in Fig. 6(a). Fig. 6(b) shows the computed edge map. Notice that the edge map contains weak edges along the LV boundary as well as spurious edges inside the LV. Fig. 6(c) shows a single contour is initialized within the LV, and Figs. 6(d)-(e) show the contour expands outward and finds the desired LV boundary. We note that applying the conventional geometric active contour described by (10) on this image failed to produce a desirable result.

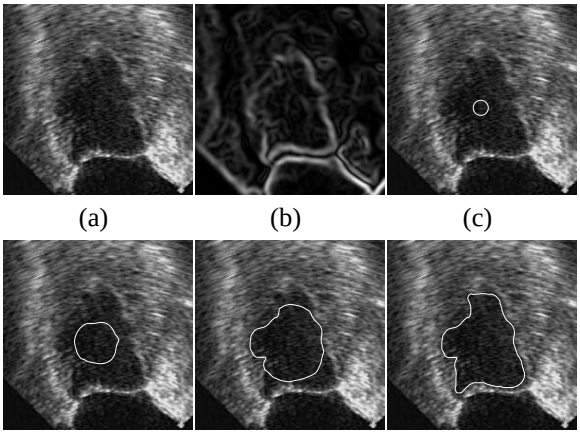

Figure 6. Segmentation of the LV on a cardiac ultrasound image from a single geometric GVF active contour. The ultrasound image of the LV (a) and its computed edge map (b). The geometric active contour expands outward and finds the LV boundary (d)-(e).

5 Conclusion

We have derived an explicit mathematical relationship between the general formulations of parametric and geometric active contours. Based on this relationship and two recent parametric active contours, we proposed two new geometric active contours. Using both simulated images and real images, we demonstrated that the new geometric active contours have flexible initialization and robust final result while addressing the boundary leaking problem faced by the conventional geometric active contours. With the explicit mathematical relationship derived in this paper, it is conceivable that additional new geometric active contours may be developed from other parametric active contours, and vice versa.

Acknowledgments

The authors would like to thank Xiao Han for providing the narrow-band implementation of the geometric active contours used in this work and Dzung Pham for providing the implementation of the fuzzy c-means algorithm. The work was supported in part by an NSF Presidential Faculty Grant (MIP93-50336) and an NIH Grant (R01NS37747).

References

[1] L. Alvarez, F. Guichard, P. L. Lions, and J. M. Morel. Axioms and fundamental equations of image processing. *Arch. Rational Mech. Anal.*, 123(3):199–257, 1993.

[2] A. A. Amini, T. E. Weymouth, and R. C. Jain. Using dynamic programming for solving variational problems in vision. *IEEE T. Patt. Anal. Mach. Intell.*, 12(9):855–867, 1990.

[3] G. Aubert and L. Blanc-Féraud. Some remarks on the equivalence between 2D and 3D classical snakes and geodesic active contours. *Int'l J. Comp. Vis.*, 34:19–28, 1999.

[4] V. Caselles, F. Catte, T. Coll, and F. Dibos. A geometric model for active contours. *Numerische Mathematik*, 66:1–31, 1993.

[5] V. Caselles, R. Kimmel, and G. Sapiro. Geodesic active contours. In *Proc. Int'l Conf. Comp. Vis.*, pages 694–699, 1995.

[6] V. Caselles, R. Kimmel, and G. Sapiro. Geodesic active contours. *Int'l J. Comp. Vis.*, 22:61–79, 1997.

[7] L. D. Cohen. On active contour models and balloons. *CVGIP: Imag. Under.*, 53(2):211–218, 1991.

[8] R. Durikovic, K. Kaneda, and H. Yamashita. Dynamic contour: a texture approach and contour operations. *The Visual Computer*, 11:277–289, 1995.

[9] M. Kass, A. Witkin, and D. Terzopoulos. Snakes: active contour models. *Int'l J. Comp. Vis.*, 1(4):321–331, 1987.

[10] S. Kichenassamy, A. Kumar, P. Olver, A. Tannenbaum, and A. Yezzi. Conformal curvature flows: from phase transitions to active vision. *Arch. Rational Mech. Anal.*, 134:275–301, 1996.

[11] B. B. Kimia, A. R. Tannenbaum, and S. W. Zucker. Shapes, shocks, and deformations I: the components of two-dimensional shape and the reaction-diffusion space. *Int'l J. Comp. Vis.*, 15:189–224, 1995.

[12] R. Malladi, J. A. Sethian, and B. C. Vemuri. Shape modeling with front propagation: a level set approach. *IEEE T. Patt. Anal. Mach. Intell.*, 17(2):158–175, 1995.

[13] T. McInerney and D. Terzopoulos. Topologically adaptable snakes. In *Proc. Int'l Conf. Comp. Vis.*, pages 840–845, 1995.

[14] T. McInerney and D. Terzopoulos. Deformable models in medical image analysis: a survey. *Med. Imag. Anal.*, 1(2):91–108, 1996.

[15] S. Osher and J. A. Sethian. Fronts propagating with curvature-dependent speed: algorithms based on Hamilton-Jacobi formulations. *J. Comp. Physics*, 79:12–49, 1988.

[16] D. Pham, J. Prince, A. Dagher, and C. Xu. An automated technique for statistical characterization of brain tissues in magnetic resonance imaging. *Int'l J. Patt. Recog. Artificial Intell.*, 11(8):1189–1211, 1997.

[17] C. S. Poon and M. Braun. Image segmentation by a deformable contour model incorporating region analysis. *Phys. Med. Biol.*, 42:1833–1841, 1997.

[18] R. Ronfard. Region-based strategies for active contour models. *Int'l J. Comp. Vis.*, 13(2):229–251, 1994.

[19] G. Sapiro and A. Tannenbaum. Affine invariant scale-space. *Int'l J. Comp. Vis.*, 11(1):25–44, 1993.

[20] K. Siddiqi, Y. B. Lauziere, A. Tannenbaum, and S. W. Zucker. Area and length minimizing flows for shape segmentation. *IEEE T. Imag. Proc.*, 7:433–443, 1998.

[21] L. H. Staib and J. S. Duncan. Boundary finding with parametrically deformable models. *IEEE T. Patt. Anal. Mach. Intell.*, 14(11):1061–1075, 1992.

[22] D. Terzopoulos and K. Fleischer. Deformable models. *The Visual Computer*, 4:306–331, 1988.

[23] C. Xu and J. L. Prince. Generalized gradient vector flow external forces for active contours. *Signal Processing — An International Journal*, 71(2):131–139, 1998.

[24] C. Xu and J. L. Prince. Snakes, shapes, and gradient vector flow. *IEEE T. Imag. Proc.*, 7(3):359–369, 1998.

[25] A. Yezzi, S. Kichenassamy, A. Kumar, P. Olver, and A. Tannenbaum. A geometric snake model for segmentation of medical imagery. *IEEE T. Med. Imag.*, 16:199–209, 1997.